Statistical Evaluation of Combined Daily Gauge Observations and Rainfall Satellite Estimates over Continental South America

DANIEL A. VILA

*Cooperative Institute of Climate Studies, and Earth System Interdisciplinary Center,
University of Maryland, College Park, College Park, Maryland*

LUIS GUSTAVO G. DE GONCALVES

*Hydrological Sciences Branch, NASA Goddard Space Flight Center, Greenbelt, and Earth System
Interdisciplinary Center, University of Maryland, College Park, College Park, Maryland*

DAVID L. TOLL

Hydrological Sciences Branch, NASA Goddard Space Flight Center, Greenbelt, Maryland

JOSE ROBERTO ROZANTE

CPTEC/INPE, Cachoeira Paulista, São Paulo, Brazil

ABSTRACT

This paper describes a comprehensive assessment of a new high-resolution, gauge–satellite-based analysis of daily precipitation over continental South America during 2004. This methodology is based on a combination of additive and multiplicative bias correction schemes to get the lowest bias when compared with the observed values (rain gauges). Intercomparisons and cross-validation tests have been carried out between independent rain gauges and different merging techniques. This validation process was done for the control algorithm [Tropical Rainfall Measuring Mission (TRMM) Multisatellite Precipitation Analysis real-time algorithm] and five different merging schemes: additive bias correction; ratio bias correction; TRMM Multisatellite Precipitation Analysis, research version; and the combined scheme proposed in this paper. These methodologies were tested for different months belonging to different seasons and for different network densities. All compared, merging schemes produce better results than the control algorithm; however, when finer temporal (daily) and spatial scale (regional networks) gauge datasets are included in the analysis, the improvement is remarkable. The combined scheme consistently presents the best performance among the five techniques tested in this paper. This is also true when a degraded daily gauge network is used instead of a full dataset. This technique appears to be a suitable tool to produce real-time, high-resolution, gauge- and satellite-based analyses of daily precipitation over land in regional domains.

1. Introduction

The spatial and temporal distribution of precipitation around the globe is needed for a variety of scientific uses, such as climate diagnostic studies and societal applications such as water management for agriculture and power, drought relief, flood control, and flood forecasting (Arkin and Xie 1994). The task of quantifying the distribution is complicated by the fact that no single, currently available estimate of precipitation has the necessary coverage and accuracy over the whole globe. Although a suite of sensors flying on a variety of satellites has been used to estimate precipitation on a global basis, generally speaking, the performance of satellite precipitation estimates over land areas is highly dependent on the rainfall regime and the temporal and spatial scale of the retrievals (Ebert et al. 2007). On the other hand, gauge observations continue to play a critical role in observations systems over global land areas. In addition, gauge observations

Corresponding author address: Daniel A. Vila, Cooperative Institute of Climate Studies (CICS), ESSIC/UMD, 2207 Computer and Space Building, College Park, MD 20742.
E-mail: dvila@essic.umd.edu

are the only source that is obtained through direct measurements. Both the radar and satellite estimates are indirect in nature and need to be calibrated or verified using the gauge observations (Xie and Arkin 1995; Ebert et al. 2007). Although it is possible to create rainfall estimates using a combination of different satellite data [i.e., Climate Prediction Center morphing technique (CMORPH); Joyce et al. 2004], researchers have increasingly moved to using "the best of both worlds" to improve accuracy, coverage, and resolution. The first such combinations were performed at a relatively coarse scale to ensure reasonable error characteristics. For example, the Global Precipitation Climatology Project (GPCP) satellite–gauge (SG) combination is computed on a monthly 2.5° × 2.5° latitude–longitude grid (Huffman et al. 1997; Adler et al. 2003), whereas finer-scale products initiated by the GPCP include the pentad (Xie et al. 2003) and one-degree daily (Huffman et al. 2001) combined estimates of precipitation.

The GPCP combination method is designed to use the strengths of each input dataset to produce merged global, monthly precipitation fields that are superior to any of the individual datasets. The technique is also designed to reduce bias in each step by using the input original or intermediate product with the presumed smallest or zero bias to adjust the bias of other products. A large-scale (5° × 5° grid box) average of the multisatellite (MS) analysis is adjusted to agree with the large-scale average of the gauges (over land and where available). This keeps the bias of the satellite and gauge combination close to the (presumably small) bias of the gauge analysis on a regional scale. Finally, the gauge-adjusted multisatellite estimate and the gauge analysis are combined with inverse-error–variance weighting to produce the final, merged analysis. This gauge–satellite combination approach allows the multisatellite estimate to provide important local variations in gauge-sparse areas while still retaining the overall gauge bias (Adler et al. 2003). In this case, the monthly gauge analysis is performed by the Global Precipitation Climatology Centre (GPCC). This gauge data is analyzed using the empirical Spheremap interpolation method (Willmott et al. 1985), which has been routinely used at the GPCC since 1991 for the calculation of grid-point results at 0.5° resolution.

The one-degree daily methodology uses GPCP retrievals by scaling the short-period estimates to sum to a monthly estimate that includes monthly gauge data (Huffman et al. 2001). A similar approach is used in Huffman et al. 2007 (hereafter H07) to scale 3-hourly estimates using the real-time TRMM Multisatellite Precipitation Analysis (TMPA), in which all available 3-hourly merged estimates are summed over a calendar month to create a monthly MS product. The MS and gauge are combined as in Huffman et al. (1997) to create a post real-time monthly SG combination. Then the field of SG/MS ratios is computed on the 0.25° × 0.25° grid (with controls) and applied to scale each 3-hourly field in the month, producing the research version, and also called version-6 3B42 product (hereafter 3B42v6).

Among multiple applications, precipitation at fine resolution along with increasing computational capacity allows for operational and research studies in hydrology across different temporal and spatial scales. However, the interaction between different scales to resolve land surface hydrology and atmospheric dynamics still needs progress and well-balanced high-resolution precipitation datasets play an essential role in such land–atmosphere interactions. One of the motivations for this paper is the potential use of high-resolution atmospheric datasets for land surface hydrology studies and numerical modeling over South America by combining surface observations with remotely sensed information. Such data fusion was made possible by the onset of Land Data Assimilation System (LDAS) initiatives (Mitchell et al. 2004; Rodell et al. 2004). A South American LDAS (SALDAS; de Goncalves et al. 2006a,b) is particularly challenging when proposing to combine high-resolution remote sensing and surface observations using land surface models (LSMs) over a continent with sparse observation networks. Precipitation (along with radiation) represents one of the most important drivers for LSMs and motivates this paper as part of the efforts of combining satellite precipitation with rain gauges for SALDAS-forcing composition and evaluation (de Goncalves et al. 2009).

This paper describes a new methodology for merging rainfall satellite estimates and daily gauge data. In this case, real-time TMPA (in which no rain gauges are incorporated) is used as a high-quality rainfall algorithm (H07), whereas the CPTEC daily rain gauge database is used to correct the bias on a daily basis over South America. Several validation tests (including cross validation and intercomparisons between rain gauge observations and satellite retrievals) have been carried out during 2004. Section 2 describes the dataset used in this paper, and section 3 presents the merging methodology. The experimental design and the validation scheme are discussed in section 4. The results and the conclusions are presented in section 5.

2. Datasets

a. Real-time TRMM Multisatellite Precipitation Analysis

This algorithm is fully described in H07. The main features of this algorithm, including the real-time adjustment,

will be outlined in this section. The first stage of the algorithm consists of the calibration and combination of microwave precipitation estimates. Passive microwave observations from the TRMM Microwave Imager (TMI), Advanced Microwave Scanning Radiometer for Earth Observing System (AMSR-E), and Special Sensor Microwave Imager (SSM/I) are converted to precipitation estimates at the TRMM Science Data and Information System (TSDIS) with sensor-specific versions of the Goddard profiling algorithm (GPROF; Kummerow et al. 1996; Olson et al. 1999), whereas Advanced Microwave Sounding Unit-B (AMSU-B) measurements are converted to precipitation estimates at the National Environmental Satellite, Data, and Information Service (NESDIS) with the operational version of the Weng et al. (2003) algorithm and corrections introduced by Vila et al. (2007). In the case of the real-time version, the calibration is made using TMI estimates from TRMM because TRMM combined instrument estimates [TCI; combines TMI and precipitation radar (PR) estimates] are not available. Also in this version, the calibration coefficients are performed using the last six available pentads (5-day period).

In a second step, the infrared precipitation estimates are created using the calibrated microwave precipitation. Histograms of time–space matched combined microwave (high-quality precipitation rates) and IR brightness temperatures (TBs), each represented on the same 3-hourly $0.25° \times 0.25°$ grid, are accumulated for one month into histograms on a $1° \times 1°$ grid, aggregated to overlapping $3° \times 3°$ windows, and then used to create spatially varying calibration coefficients that convert IR TBs to precipitation rates. In the final stage, the microwave and IR estimates are combined. The physically based combined microwave estimates are taken ''as is'' where available, and the remaining grid boxes are filled with microwave-calibrated IR estimates. A detailed description of this algorithm can be found in H07. The daily accumulation is obtained summing the individual 3-h files from 1500 UTC of the previous day (1200–1500 UTC period) to 1200 UTC (0900–1200 UTC period) of the current day.

b. Rain gauge database

The data sources for the daily surface precipitation observations used, in addition to those of the World Meteorological Organization (WMO), are obtained through an Instituto Nacional de Pesquisas Espaciais (INPE) compilation of the following agencies: (i) Agência Nacional de Energia Eléctrica (ANEEL; National Agency For Electrical Energy); (ii) Agência Nacional de Águas (ANA; National Water Agency); (iii) Fundação Cearense de Meteorologia e Recursos Hídricos (FUNCEME; Meteorology and Hydrologic Resources Foundation of Ceará); (iv) Superintendência do Desenvolvimento do Nordeste (SUDENE; Superintendency for the Development of the Northeast); and (v) Departamento de Águas e Energia Elétrica do Estado de São Paulo (DAEE; Department of Water and Electrical Energy for the State of São Paulo) in collaboration with the Centro de Previsão de Tempo e Estudos Climáticos (CPTEC; Brazilian Weather Forecast and Climate Studies Center) and (vi) the Technological Institute of Paraná (SIMEPAR). Figure 1 shows the available daily rain gauge observations for 26 March 2004. Most of the available stations are located along the Brazilian coast, where the most influential cities of Brazil are located, whereas other countries such as Colombia and Venezuela have less than 10 rain gauge reports each for this particular day. The rain gauges spatial distribution is similar all around the year with 900–1300 reports per day. In all cases, the accumulation time is from 1200 UTC of the previous day to 1200 UTC of the current day. It is important to point out that with the additional observations from local South American agencies and Brazilian automated weather stations, the number of observations in the CPTEC/INPE database is somewhat 4 times larger than in GPCC datasets. This addition will help to retain the overall gauge bias at finer scales.

3. Merging methodology

The determination of the methodology for constructing a merging technique for daily rainfall estimates over land using a satellite-based algorithm and rain gauge network involves three major issues: 1) define the algorithm to be used in the merging process; 2) design the merging technique; and 3) define an validation strategy to assess the results.

With regard to the first issue, the experimental real-time daily TMPA (TMPA-RT; H07) is used as the base algorithm for retrieving precipitation because TMPA is successful at approximately reproducing the surface observation–based histogram of precipitation (3B42RT), as well as reasonably detecting large daily events, although it does not include information from rain gauges (control algorithm).

The second issue has been largely discussed in several papers over the years. In most cases, the SG estimate is computed on a monthly basis (Xie and Arkin 1997; Adler et al. 2003). The Climate Precipitation Center Merged Analysis of Precipitation (CMAP; Xie and Arkin 1997) approach uses a blended technique developed by Reynolds (1988), in which the combined satellite estimates and the gauge data are combined to
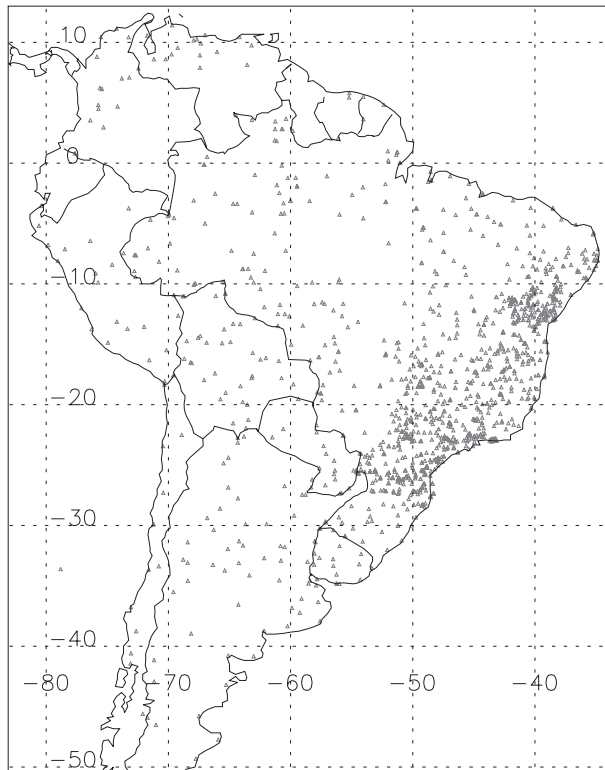
FIG. 1. Daily rainfall reports received on 26 Mar 2004 over South America. This figure includes data from different Brazilian agencies compiled at INPE.

define the relative distribution and the absolute value of the precipitation field, respectively. On the other hand, the GPCP approach (Huffman et al. 1997; Adler et al. 2003) has been adopted for a different approach as described in section 1. The CMAP approach also was applied for pentad precipitation analysis (Xie et al. 2003), whereas a variant of the GPCP strategy was applied by H07 to create a 3-hourly, $0.25° \times 0.25°$ grid analysis (see introduction).

In all cases, generally speaking, there exists the assumption that the rain gauge observations have lower bias, so this information will prevail over any satellite retrievals in those regions with more dense networks, whereas over the ocean (not analyzed in this paper) and non well-gauged areas, the multisatellite estimates have a larger weight in the final analysis.

In the proposed approach, daily gauge observations will be used instead of monthly accumulations. The irregular spatial distribution of rain gauges over the target region (Fig. 1) makes daily gauge analysis a very challenging issue. A recent study (Chen et al. 2008) shows the assessment of different objective techniques for gauge-based analysis in several regions around the world. Over South America, such techniques show a good perfor-

mance, whereas in other regions such as Africa where the gauges are sparser, these techniques cannot satisfactorily represent the daily rainfall field.

On the other hand, short-time rainfall (i.e., daily accumulation) is much more variable than monthly precipitation, so regional effects like topography and local circulation play an important role in rainfall generation that need that can be smoothed into monthly scales. To address this issue, the proposed correction technique is based on (i) additive and (ii) multiplicative bias correction schemes applied for each station on a daily basis. With the first scheme, the observed value (gauge station) is subtracted from the satellite rainfall retrieval, whereas with the second scheme, the ratio between the observed and estimated value is performed. Those station-based bias values are gridded using an inverse-distance weight algorithm (with controls) to fit the multisatellite estimate resolution ($0.25°$, in this case). Although the multiplicative scheme suggests that the ratio between the observed and estimated value is suitable to remove the bias of satellite retrievals on daily basis, this methodology is not useful for determining the magnitude of the precipitation when the retrieved satellite value is zero and the observed value is different from zero (i.e., warm clouds and/or clouds with no ice structure). On the other hand, additive correction schemes produce large differences when large discrepancies exist between the observed and estimated values and the probability density function (PDF) does not fit with observed values.

The proposed scheme [hereafter combined scheme (CoSch)] uses three steps to combine those two approaches into a single method and remove the bias of satellite estimates that overcomes some limitations of both schemes used separately.

The additive bias correction (ADD) is defined as follows:

$$rr^+ = rr_{sat} + \overline{(rr^i_{obs} - rr^i_{sat})}, \qquad (1)$$

where rr_{sat} are the multisatellite-based retrieval and $\overline{(rr^i_{obs} - rr^i_{sat})}$ represent the result of gridding (represented by the bar) the additive bias between the observed rainfall and the satellite retrieval (3B42RT, in this case) for each station (denoted by the superscript i).

Similar to the previous equation, the ratio bias correction (RAT) is defined as follows:

$$rr^* = rr_{sat} \times \overline{\left(\frac{rr^i_{obs}}{rr^i_{sat}}\right)}, \qquad (2)$$

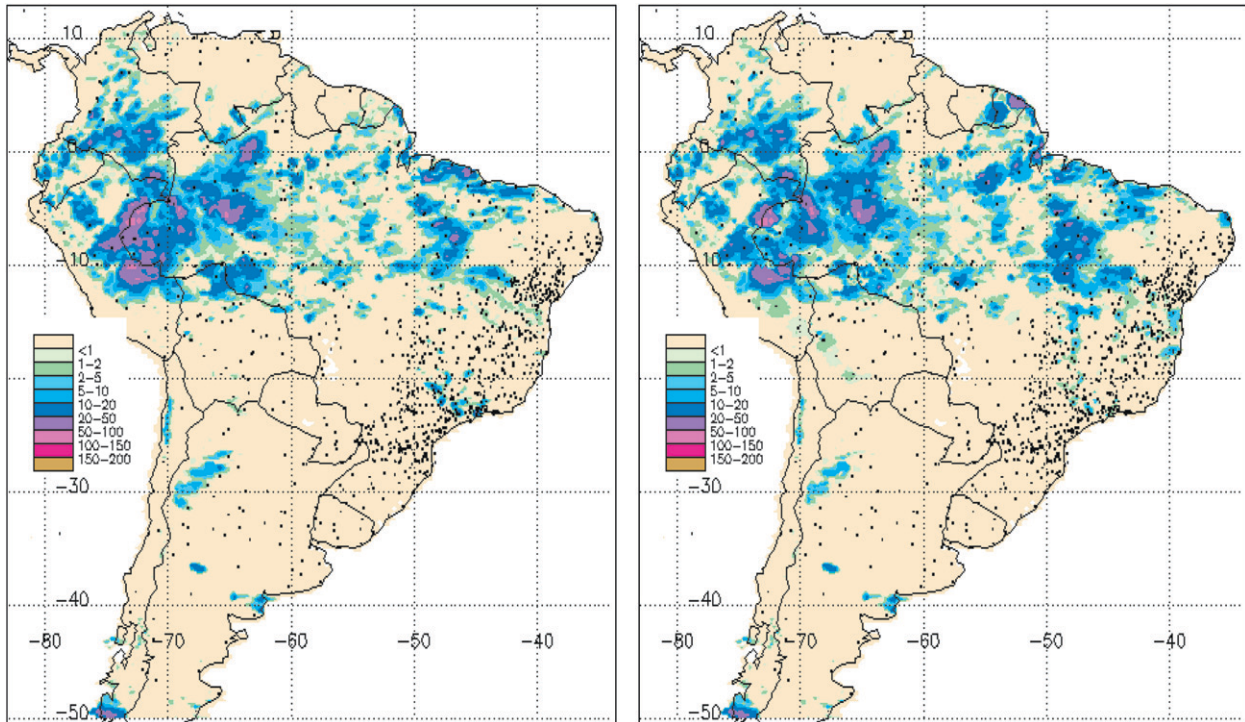where the same conventions as in ADD [Eq. (1)] were used.

FIG. 2. Rainfall retrieval on 26 Mar 2004 for (left) 3B42RT and (right) after applying CoSch.

After this procedure, the first step is to interpolate the rain gauge observations using the nearest neighbor method (original values are retained), masking out all regions with a distance greater than five grid points from the closest station. In this case, the grid size is 0.25° to match the satellite estimates.

In a second step, the difference between additive/multiplicative bias correction and observed values (defined in the previous step) is performed. One particular scheme (additive or multiplicative) is selected for each grid point based on the minimum difference between that particular bias correction and the observation. For each nonmasked grid point, one particular method is assigned.

In the third step, the bias-corrected rainfall is defined as follows: the multisatellite (3B42RT) estimate remains with no correction in those areas masked out in the first step of the procedure. The bias-corrected rainfall in the rest of the land areas is defined as a weight average of the additive and multiplicative bias correction schemes as follows:

$$\mathrm{rrcorr}_i = \alpha \times \mathrm{rr}_i^+ + \beta \times \mathrm{rr}_i^*, \qquad (3)$$

where rrcorr is the final result for the CoSch scheme. Here, rr^+ and rr^* are defined in (1) and (2) (in this case, the subscript i denotes a particular grid point), and α and β are the weight factors. These weight factors represent the number of times a particular scheme is selected

in a 3° × 3° box centered in the grid box with i divided by the total grid points in that particular box (excluded all masked points). By construction, $\alpha + \beta = 1$ for every nonmasked grid point. This approach takes into account large-scale variations (in terms of which scheme works better in a larger area than a single grid point) and also produce spatially continuous rainfall fields.

Figure 2 shows the rainfall field for 26 March 2004 for 3B42RT (left panel) and after applying the CoSch scheme (right panel). Although the general spatial pattern is preserved in both retrievals, some differences in absolute value are observed in the western Amazonia and French Guyana (among others smaller regions) based on ground observations. Figure 3a shows the relative PDF distribution (in percent) for this particular day. It is observed that the relative PDF distribution for both retrievals (before and after the bias correction) shows a similar structure. In a broader perspective, the relative PDF distribution (in percent) for 2004 is also presented (Fig. 3b). In this case, the gauge-based PDF is also included in the same graph. This histogram exhibits a similar shape for all considered variables (multisatellite, merge analysis, and individual observations).

To assess the temporal continuity of this bias correction scheme, January 2004 (Southern Hemisphere summer) was selected to determine if any correction scheme shows some preference over the other over
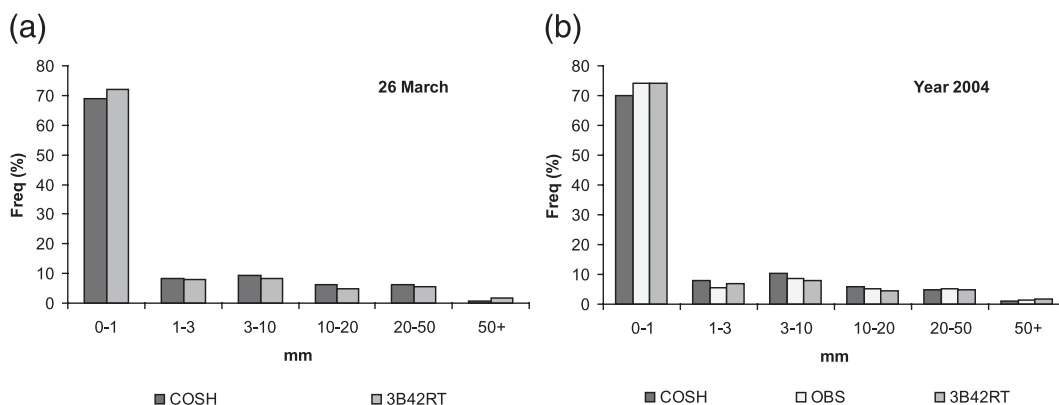
(a)

(b)

FIG. 3. (a) Relative PDF distribution (%) for CoSch and 3B42RT on 26 Mar 2004. (b) Same as (a) but for 2004 and the observed rainfall PDF is also included.

time. Figure 4 shows the percentage of pixels, for a given day, that a certain correction scheme was selected. The result shows a pretty steady situation during the month in which around 54% of the pixels are selected according to the ADD scheme, whereas only 46% of the time the RAT technique is chosen. Considering the mentioned values for both schemes, the difference between the number of days (in percent) that a given scheme was chosen and the mean value for January 2004 was calculated for techniques (ADD and RAT). The spatial distribution of RAT relative bias (percentage of days above or below the average defined in the previous sentence) is presented in Fig. 5a. Because of construction constrains, the sum of RAT and ADD (not shown) is equal to 0. It can be observed that over southern South America (approximately southward 20°S), the RAT scheme is selected approximately 20% above the average (bluish colors), whereas this behavior is opposite over most of part of the Brazilian territory and Bolivia, where reddish colors prevail. This means that RAT is less frequently selected than the average, so ADD scheme is more frequently selected during this particular month. The largest deviations from the average are observed along the coasts of Chile, Peru, Colombia, Venezuela, and the Guyanas. Those regions exhibit the scarcest gauge networks in the region. One hypothesis about this behavior is that the selection of a given scheme is related to the precipitation regime. Figure 5b shows a close agreement between the RAT bias and the accumulated monthly rainfall: larger values of rainfall are associated with negative (positive) values of RAT (ADD), whereas RAT (ADD) is more (less) frequently chosen in those regions with less (more) rainfall. Other factors such as circulation and gauge density (see Fig. 1) also should influence these results, but this discussion is out of the scope of this research.

The third issue, about the validation strategy, will be described in the next section.

4. Validation strategy and experimental design

For testing this bias removal technique, a daily rain gauge dataset for South America during 2004 (refer to section 2b for more details) was used in two ways in a cross-correlation process: (i) gauge reports show 10% of the randomly selected stations were withdrawn; and (ii) those at the remaining 90% of the stations were used in the bias removal process. This cross correlation process was conducted systematically 10 times but every time the validation dataset (10%) is selected from the remaining data used in the previous step. This process guarantees that each gauge was withdrawn once. The corrected rainfall estimate was then compared with the corresponding observation to examine the performance of the proposed technique. This process is similar to the methodology described in Chen et al. (2002, 2008). For
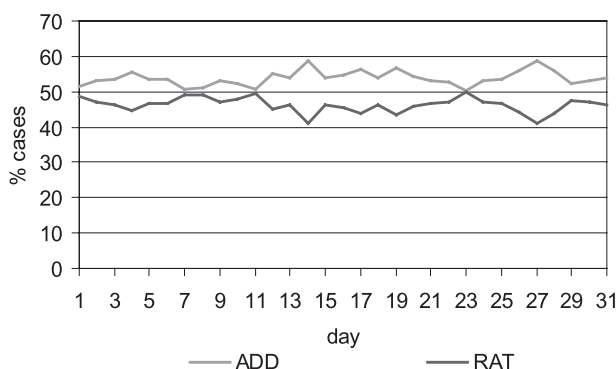

FIG. 4. Percentage of pixels selected for both bias removal procedures for January 2004. Uncorrected and no-rainfall pixels are excluded in this analysis.
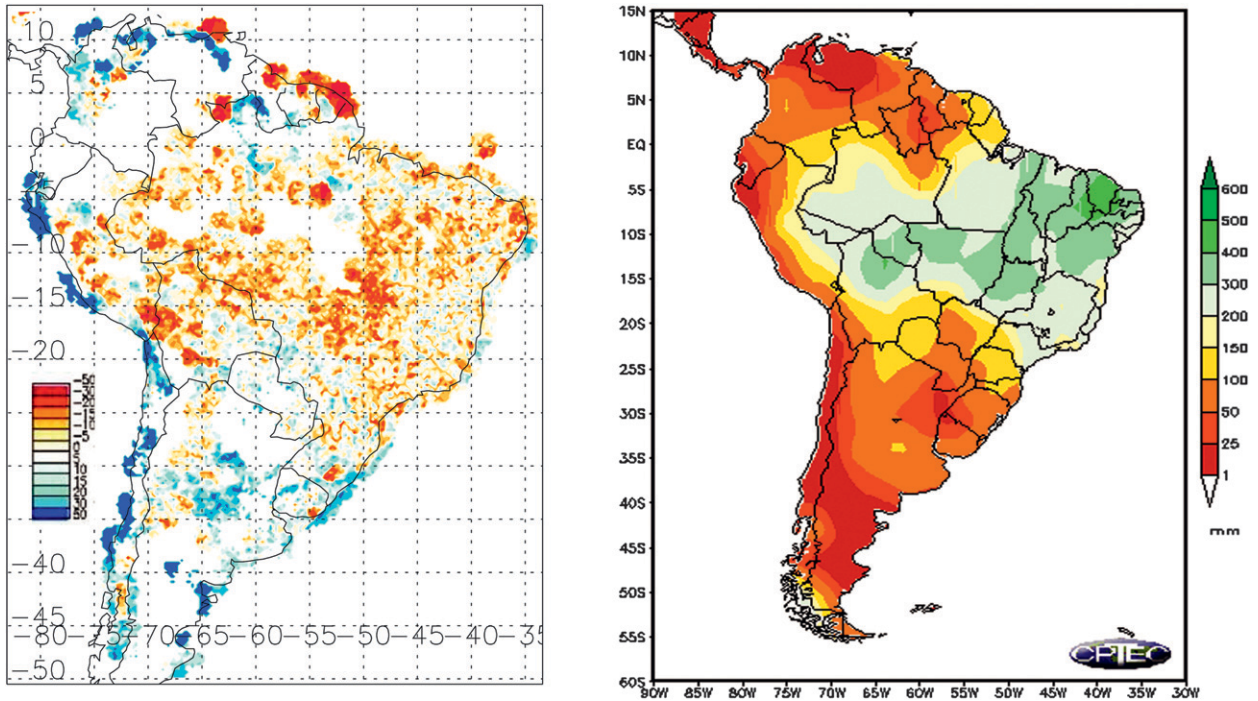
FIG. 5. (left) Spatial distribution of RAT relative bias for January 2004. Positive values (blues) mean that RAT was chosen above 46% (average value) of the time, whereas negative values (reds) show the opposite behavior. (right) Monthly rainfall accumulation for January 2004 (data available online at http://www.cptec.inpe.br/clima/).

comparison purposes, four other estimates were included in this study: additive bias removal and ratio bias removal (as defined in the previous section) and the research and real-time version of TMPA (3B42V6 and 3B42RT). For the first two correction schemes (ADD and RAT), the same cross correlation process is performed; however, for the last two estimates, the values of 3B42V6 and 3B42RT (control run) were selected and compared for the same validation dataset (10% of rain gauges randomly selected and conducted 10 times) to make all the statistical results comparable among them. Table 1 shows the monthly mean (calculated on daily basis from individual measurements) of bias (in millimeters), root-mean-square error (in millimeters), and correlation coefficient (CORR) for the five proposed models for January, April, July, and October 2004. Bold values are the best result obtained for a particular month and for each statistical parameter. In this case, it can be shown that the CoSch has a better performance than ADD and RAT separately, but it also has a better performance than 3B42V6. This situation is highly remarkable when RMSE and CORR are compared among different estimates. Among these five different estimates, the worse performance is for 3B42RT (control algorithm), in which no rain gauge information is added. This result shows that the CoSch adds some extra value to the ADD and RAT when used separately, retaining some local spatial variability on daily rainfall.

In 2003 the International Precipitation Working Group (IPWG) began a project to validate and intercompare

TABLE 1. Cross-validation test results over South America for January, April, July, and October using 90% of gauge network for the bias removal process in CoSch, ADD, and RAT. Best results for each month are in bold.

|	3B42RT			CoSch			ADDITIVE			RATIO			2B42V6		
	BIAS (mm)	RMSE (mm)	CORR	BIAS (mm)	RMSE (mm)	CORR	BIAS (mm)	RMSE (mm)	CORR	BIAS (mm)	RMSE (mm)	CORR	BIAS (mm)	RMSE (mm)	CORR
January	−0.65	9.15	0.38	**−0.22**	**6.70**	**0.57**	0.37	8.71	0.44	0.37	8.71	0.44	0.24	8.61	0.43
April	0.18	5.29	0.34	**−0.14**	**3.78**	**0.51**	0.60	4.87	0.38	0.25	4.87	0.38	0.03	4.88	0.38
July	−0.36	2.95	0.27	**−0.22**	**1.84**	**0.51**	1.05	2.83	0.31	−0.17	2.83	0.31	−0.31	2.86	0.33
October	1.05	4.32	0.35	**0.05**	**3.04**	**0.47**	0.25	4.23	0.41	1.27	4.23	0.41	1.21	4.22	0.38
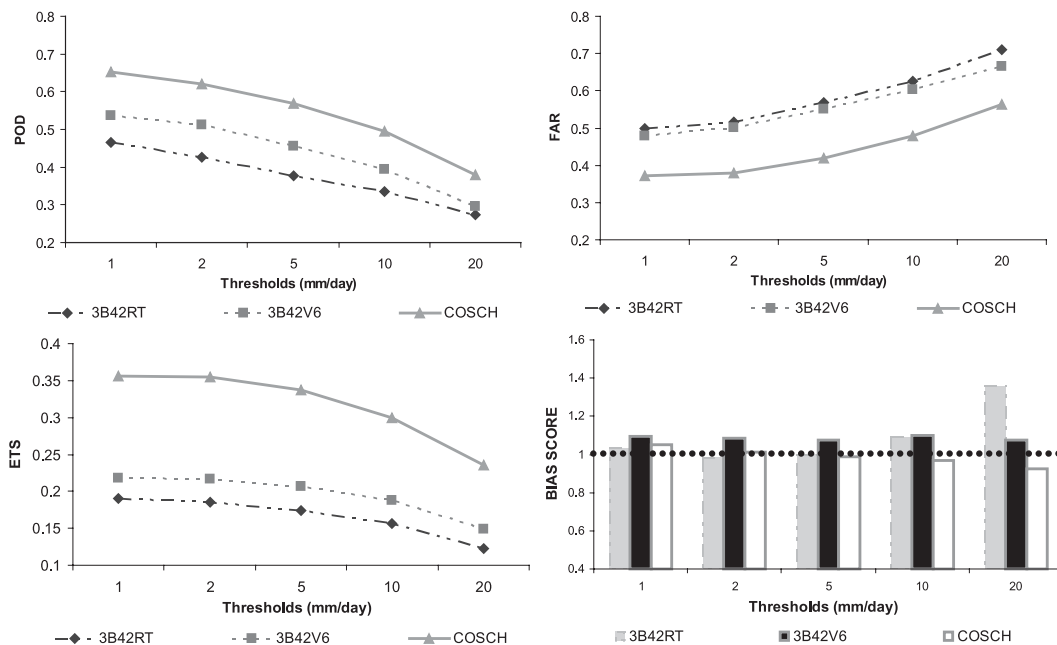
FIG. 6. Annual mean of POD, FAR, ETS, and BIAS for different rainfall thresholds. Here, 90% of gauge network was used to perform CoSch.

satellite rainfall estimates (Ebert et al. 2007). Some categorical statistics such as bias score (BIAS), probability of detection (POD), false alarm ratio (FAR), and equitable threat score (ETS) can be computed for different rain rate thresholds as follows: 1, 2, 5, 10, 20, and 50 mm. All these parameters can be computed from a rain/no-rain contingency table and measure the performance of a given algorithm (refer to Wilks 1995 for more details). Figure 6 shows the annual mean of the aforementioned categorical statistics (based on daily estimates) for 3B42RT, 32B42V6, and CoSch for all rainfall thresholds, except for 50 mm because the lack of events above that threshold can affect the robustness of the statistics. It can be shown that the performance of CoSch is better for all rainfall thresholds. POD (Fig. 6a) is higher for all thresholds, suggesting that CoSch can get more correct estimates in each category, whereas FAR (Fig. 6b) is smaller for all categories, suggesting that the amount of false alarms estimated by CoSch is smaller than other estimates. BIAS (Fig. 6c) shows similar values for all estimates (close to one, which is the ideal value). Nevertheless, CoSch tends to overestimate lower values and underestimate the largest values. ETS (Fig. 6d) measures the fraction of observed and/or estimated events that were correctly estimated, adjusted for hits associated with random chance. This parameter is sensitive to hits because it penalizes both misses and false alarms in the same way. In this case, the improvement is clear for all rainfall thresholds when compared with 3B42RT and 3BR2V6.

To further quantify the influence of the gauge network density on the accuracy of all different estimates, cross-validation tests were conducted using only 10% (randomly selected) of available data to perform the additive, ratio, and the combined schemes. Another 10% (excluding those chosen to perform the correction) was used to validate the results of the aforementioned schemes and also 3B42RT and 3B42V6. This experiment was carried out 10 times using the same strategy as the previous analysis. This approach guarantees that each gauge was withdrawn once. Both results, using 90% of the gauges in the first analysis and using only 10% to perform the correction in a second experiment, are statistically comparables. This comparison gives us the opportunity to examine the influence of varying gauge density to the quantitative accuracy of the methodology. Table 2 shows the same statistical parameters as Table 1 but, in this case, with only 10% of the gauges being used to perform the bias removal process. As expected, the performance of these methodologies (CoSch, ADD, and RAT) improves with increasing density of the gauge network, whereas the other estimates (3B42RT and 3B42V6) show approximately the same values because the number of gauges used to validate remains the same (10% randomly selected for each of the 10 experiments). Nevertheless, it is important to point out that despite using 10% of available gauges to compute the bias removal process, the technique shows similar results as 3B42V6 (which uses high-quality monthly data to perform

TABLE 2. Same as Table 1 but using only 10% of gauges.

	3B42RT			CoSch			ADDITIVE			RATIO			2B42V6		
	BIAS (mm)	RMSE (mm)	CORR	BIAS (mm)	RMSE (mm)	CORR	BIAS (mm)	RMSE (mm)	CORR	BIAS (mm)	RMSE (mm)	CORR	BIAS (mm)	RMSE (mm)	CORR
January	−0.75	9.09	0.38	**0.99**	**8.38**	**0.47**	1.07	8.46	0.47	2.12	9.99	0.41	0.15	8.63	0.44
April	**0.14**	5.21	0.32	0.37	**4.70**	**0.39**	0.31	4.95	0.38	0.41	5.21	0.34	0.16	4.89	0.37
July	−0.44	3.02	0.26	**−0.03**	**2.38**	**0.42**	0.43	2.59	0.41	−0.44	2.74	0.28	−0.34	2.84	0.33
October	0.97	4.36	0.36	0.97	**4.07**	0.39	**0.76**	4.14	0.39	1.53	4.71	0.34	1.19	4.21	**0.40**

a bias removal process, as explained in section 2) and 3B42RT. On the other hand, CoSch performed better than ADD and RAT separately. In this case, the difference between CoSch and RAT and between CoSch and ADD is closer than in the previous analysis, suggesting that, for very sparse rain gauge networks, the added value of the combination is less effective than in the previous case. A similar situation can be observed with the rest of the categorical statistics (Fig. 7). The performance of CoSch is better for all the rainfall thresholds, but the difference, as expected, is smaller than the previous analysis. The POD (Fig. 7a) is higher for all thresholds, suggesting that despite the network density being very scarce, CoSch can get more correct estimates in each category, whereas FAR (Fig. 7b) is smaller, suggesting that fewer false alarms are estimated by CoSch in all categories than other estimates. The BIAS (Fig. 7c) shows similar values for all estimates (close to one, which is the ideal value), whereas ETS

(Fig. 7d) shows an improvement for all the rainfall thresholds when compared with 3B42RT and 3BR2V6.

5. Summary and conclusions

A comprehensive assessment has been performed to examine the performance of a new methodology (CoSch) to merge satellite estimates and daily gauge data over South America during 2004. For comparison purposes, 3B42RT (control algorithm) and 3B42V6 (which also include calibrated monthly gauge data from GPCC) were also included in this analysis. Two intermediate results (ADD and RAT) used in the combined scheme were also examined to determine how the proposed methodology works.

Intercomparisons and cross-validations tests have been carried out for the control algorithm and for the different merging schemes over a South American region during 2004, for different months belonging to
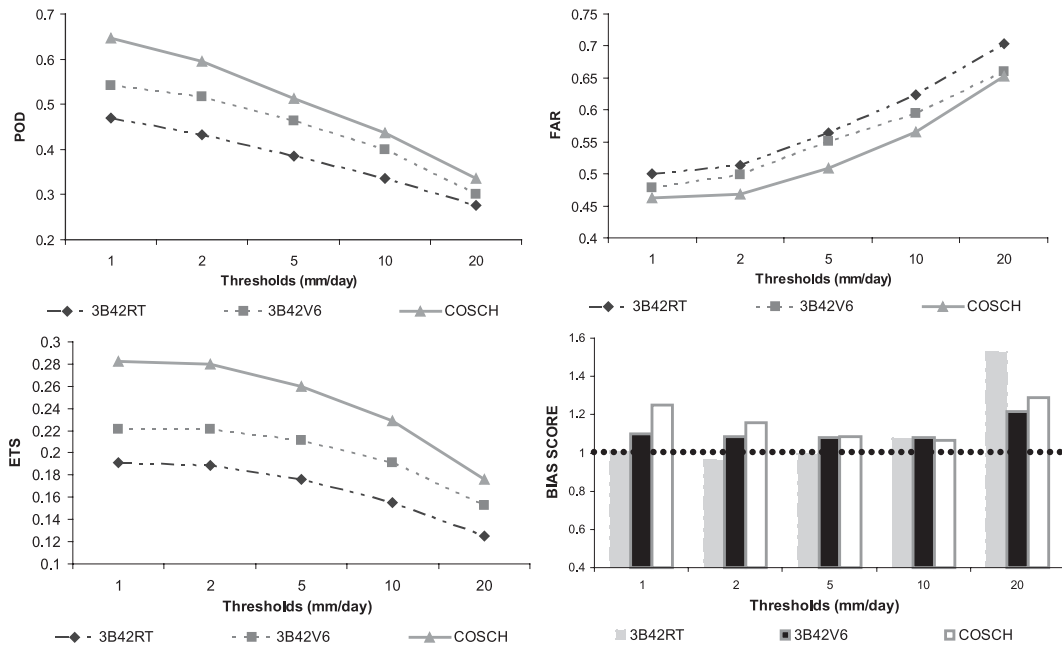

FIG. 7. Same as Fig. 3 but with 10% of gauge network used to perform CoSch.

different seasons and for different network densities. The results are summarized as follows:

- The election of the bias removal technique seems to be related to the rainfall regime: the additive bias correction scheme is selected above the mean value when the rainfall rate is lower and the inverse case occurs with the ratio-based scheme.
- The RMSE and the correlation coefficient of the CoSch performs better than ADD and RAT separately, suggesting that an extra value is added when the proposed scheme is used. CoSch also shows the best results of all analyzed merged schemes.
- The control algorithm (3B42RT) presents the poorest performance. This result is expected because this algorithm does not use any gauge data, whereas 3B42V6, which includes only the GPCC monthly data, tends to improve all statistic parameters when compared with 3B42RT, using an independent gauge dataset to validate.
- In term of the performance for different rainfall thresholds, CoSch again shows the best performance when compared with other merging techniques and the control run.
- The quality of the rainfall estimate degrades as the gauge network being used became sparser. Nevertheless, the retrieval has almost the same quality (from a statistical point of view) as those based on monthly gauge data.

Based on these results, future work will be focused on the evaluation of this technique under different rainfall regimes and on a different region of the world. This experience could be replicated using different control algorithms (i.e., CMORPH) to provide the scientific community with a suite of high-resolution, high-quality satellite–gauge-based analyses of daily precipitation over land in global and regional domains. Nonetheless, because the high-resolution precipitation datasets constrained by daily observations are suitable for land surface and weather application, this technique has been identified as one of the best candidates for precipitation data forcing production for the South American LDAS across the entire continent.

It is also important to mention that other factors like instrumental errors (e.g., wind blowing, wall wetting, evaporation, and splashing, among others) can also affect the precipitation measurement but the analysis of those factors are out of the scope of this paper.

REFERENCES

Adler, R. F., and Coauthors, 2003: The Version-2 Global Precipitation Climatology Project (GPCP) Monthly Precipitation Analysis (1979–present). *J. Hydrometeor.,* **4,** 1147–1167.

Arkin, P. A., and P. Xie, 1994: The Global Precipitation Climatology Project: First Algorithm Intercomparison Project. *Bull. Amer. Meteor. Soc.,* **75,** 401–419.

Chen, M., P. Xie, J. E. Janowiak, and P. A. Arkin, 2002: Global land precipitation: A 50-yr monthly analysis based on gauge observations. *J. Hydrometeor.,* **3,** 249–266.

——, W. Shi, P. Xie, V. B. S. Silva, V. E. Kousky, R. Wayne Higgins, and J. E. Janowiak, 2008: Assessing objective techniques for gauge-based analyses of global daily precipitation. *J. Geophys. Res.,* **113,** D04110, doi:10.1029/2007JD009132.

De Goncalves, L. G. G., J. Shuttleworth, S. C. Chou, Y. Xue, P. Houser, D. Toll, J. Marengo, and M. Rodell, 2006a: Impact of different initial soil moisture fields on Eta model weather forecasts for South America. *J. Geophys. Res.,* **111,** D17102, doi:10.1029/2005JD006309.

——, W. J. Shuttleworth, E. J. Burke, P. Houser, D. L. Toll, M. Rodell, and K. Arsenault, 2006b: Toward a South America Land Data Assimilation System: Aspects of land surface model spin-up using the Simplified Simple Biosphere. *J. Geophys. Res.,* **111,** D17110, doi:10.1029/2005JD006297.

——, and Coauthors, 2009: The South American Land Data Assimilation System (SALDAS) 5-Year Retrospective Atmospheric Forcing Datasets. *J. Hydrometeor.,* in press.

Ebert, E. E., J. E. Janowiak, and C. Kidd, 2007: Comparison of near-real-time precipitation estimates from satellite observations and numerical models. *Bull. Amer. Meteor. Soc.,* **88,** 47–64.

Huffman, G. J., and Coauthors, 1997: The Global Precipitation Climatology Project (GPCP) combined precipitation dataset. *Bull. Amer. Meteor. Soc.,* **78,** 5–20.

——, R. F. Adler, M. Morrissey, D. T. Bolvin, S. Curtis, R. Joyce, B. McGavock, and J. Susskind, 2001: Global precipitation at one-degree daily resolution from multisatellite observations. *J. Hydrometeor.,* **2,** 36–50.

——, and Coauthors, 2007: The TRMM Multisatellite Precipitation Analysis (TMPA): Quasi-global, multiyear, combined-sensor precipitation estimates at fine scales. *J. Hydrometeor.,* **8,** 38–55.

Joyce, R. J., J. E. Janowiak, P. A. Arkin, and P. Xie, 2004: CMORPH: A method that produces global precipitation estimates from passive microwave and infrared data at high spatial and temporal resolution. *J. Hydrometeor.,* **5,** 487–503.

Kummerow, C., W. S. Olson, and L. Giglio, 1996: A simplified scheme for obtaining precipitation and vertical hydrometeor profiles from passive microwave sensors. *IEEE Trans. Geosci. Remote Sens.,* **34,** 1213–1232.

Mitchell, K. E., and Coauthors, 2004: The multi-institution North American Land Data Assimilation System (NLDAS): Utilizing multiple GCIP products and partners in a continental distributed hydrological modeling system. *J. Geophys. Res.,* **109,** D07S90, doi:10.1029/2003JD003823.

Olson, W. S., C. D. Kummerow, Y. Hong, and W.-K. Tao, 1999: Atmospheric latent heating distributions in the tropics derived from satellite passive microwave radiometer measurements. *J. Appl. Meteor.,* **38,** 633–664.

Reynolds, R. W., 1988: A real-time global sea surface temperature analysis. *J. Climate,* **1,** 75–87.

Rodell, M., and Coauthors, 2004: The Global Land Data Assimilation System. *Bull. Amer. Meteor. Soc.,* **85,** 381–394.

Vila, D., R. Ferraro, and R. Joyce, 2007: Evaluation and improvement of AMSU precipitation retrievals. *J. Geophys. Res.,* **112,** D20119, doi:10.1029/2007JD008617.

Weng, F., L. Zhao, R. Ferraro, G. Poe, X. Li, and N. Grody, 2003: Advanced microwave sounding unit cloud and precipitation algorithms. *Radio Sci.,* **38,** 8068–8079.

Wilks, D. S., 1995: *Statistical Methods in the Atmospheric Sciences: An Introduction.* Academic Press, 467 pp.

Willmott, C. J., C. M. Rowe, and W. D. Philpot, 1985: Small-scale climate maps: A sensitivity analysis of some common assumptions associated with grid-point interpolation and contouring. *Amer. Cartogr.,* **12,** 5–16.

Xie, P., and P. A. Arkin, 1995: An intercomparison of gauge observations and satellite estimates of monthly precipitation. *J. Appl. Meteor.,* **34,** 1143–1160.

——, and ——, 1997: Global precipitation: A 17-year monthly analysis based on gauge observations, satellite estimates, and numerical model outputs. *Bull. Amer. Meteor. Soc.,* **78,** 2539–2558.

——, J. E. Janowiak, P. A. Arkin, R. Adler, A. Gruber, R. Ferraro, G. J. Huffman, and S. Curtis, 2003: GPCP pentad precipitation analyses: An experimental dataset based on gauge observations and satellite estimates. *J. Climate,* **16,** 2197–2214.